Available online at www.sciencedirect.com

ScienceDirect

Procedia Structural Integrity 13 (2018) 1583–1588

Structural Integrity Procedia

www.elsevier.com/locate/procedia

ECF22 - Loading and Environmental effects on Structural Integrity

Low-cycle fatigue hysteresis by thermographic and digital image correlation methodologies: a first approach

Guido La Rosa, Carmelo Clienti, Adriana Marino Cugno Garrano, Fabio Lo Savio

DICAR, University of Catania, Via S. Sofia 64, 95123 Catania, Italy

Abstract

The energetic behaviour of the material under low-cycle fatigue (LCF) can be controlled by the hysteresis cycle in order to define the variation of the mechanical characteristics and to forecast the fatigue and the failure response. The traditional analysis is performed using the force-displacement signals derived by the testing machine that can be coupled with other measuring methodologies. In the present paper, the authors have used the Digital Image Correlation (D.I.C.) to better define the specimen displacement, avoiding many errors of the displacement measurement chain. The thermographic analysis (T.A.), able to follow quickly and with great accuracy the energetic variations, was combined with the stress-strain measurements, allowing to calculate the damping energy. The results pointed out a similar behaviour between the hysteresis areas defined basing on the D.I.C. displacements and those found by the testing machine outputs, but substantial differences in terms of values. The thermal variations and the areas of the hysteresis loops, both linked to the plastic energy, were compared, showing a reliable agreement.

Peer-review under responsibility of the ECF22 organizers.

Keywords: Low-cycle fatigue; Hysteresis; Digital Image Correlation (D.I.C.); Thermography.

1. Introduction

The fatigue phenomenon is provoked by the crack nucleation and propagation, together with the production of plastic energy, increasing with the fracture growth. It has been shown that the thermographic analysis enables an assessment and prediction of the fatigue life based on the analysis of the surface radiometric temperature irradiated from specimens or mechanical components subjected to cyclic loading (Boulanger et al. 2004, Giancane et al. 2009, Charkaluk and Constantinescu 2009, Crupi et al. 2010 and 2011, Naderi et al. 2010, Plekhov et al. 2007, La Rosa and Risitano 2000, Risitano et al. 2015, Kaleta et al. 1990, Luong 1988, Meneghetti et al. 2013, La Rosa et al. 2014) and how this measurement is sensitive to the damage of the component itself. Most of these are based on the acquisition and assessment of the energy response of the material subjected to cyclic or combined trains of cycles loading; these allow the prediction of the main parameters of the fatigue response such as, as an example, the fatigue limit, the duration of the fatigue lifetime (Fargione et al. 2002) and the damage (Curà and Gallinati 2011, Risitano and Risitano 2010 and 2013, Grover 1960).

2452-3216
Peer-review under responsibility of the ECF22 organizers.
10.1016/j.prostr.2018.12.323

Nomenclature

A hysteresis area
A_{DIC} hysteresis area calculated by the D.I.C. analysis
A_{mach} hysteresis area calculated by the testing machine parameters
ΔT thermal variation
σ_0 maximum stress in monoaxial loading
ε_0 maximum strain in monoaxial loading
φ phase angle between stress and strain
φ_{DIC} phase angle between stress and strain calculated by D.I.C.
φ_{mach} phase angle between stress and strain calculated by the testing machine parameters
ε_{0DIC} maximum strain by D.I.C.
ε_{0mach} maximum strain by the testing machine parameters
R loading ratio (R = minimum load/maximum load)

On the other hand, the progress of the damage can be warned by the analysis of the cyclic curve showing, at each cycle, the growth of the area of hysteresis with the reached peak stress. This area can be easily calculated by recording the testing machine outputs in terms of applied load and displacement. Even if the load can be precisely measured by the load cell, the displacement is affected by many errors in the loading chain (clearances, cross-head deformations, slips of the specimen on the grips, etc.). The measurement of the deformation of the specimen must be carefully carried out by other techniques as extensometers, strain gauges (mechanical, electrical or optical), image analysis systems.

The thermal energy does not depend only on the plastic energy correlated with the damping of the material and, consequently, on the hysteresis loop. This is nevertheless indicative of the material fatigue as well as the temperature detected by remote sensing thermal measurements (Felter and Morrow 1961, Audenino et al. 2003, Roy et al. 2013).

Based on the previous researches (Kanchanomai et al. 2002, Dattoma et al. 2013, Hunadi et al. 2012, Sarkar et al. 2014, Tao and Xia 2005, Giancane et al. 2010, Wattrisse et al. 2001, Li et al. 2016), the authors present their first experiences in the analysis of the fatigue phenomenon by combined thermographic analysis (T.A.) and digital image correlation (D.I.C.) methodologies. Due to the previous results, they used an accelerated technique based on pulses trains at low number of cycles to determine the thermal response as well as the D.I.C. deformation measurements.

2. Description of the investigation

The tests were carried out by recording contemporaneously the force-displacement information derived by the testing machine, the D.I.C. images and the thermal maps. The experimental setup is shown in Figures 1 and 2, placing the thermocamera and the videocamera (for the D.I.C. analysis) face to face respect the flat specimen mounted on the testing machine. The flat steel specimens were treated on both the surfaces: on one side (T.A.) the samples were covered by black paint, in order to increase the thermal emissivity and to reduce the reflected energy; on the other side (D.I.C.), after painting the surface of white, black dots were sprayed on the samples by airbrush to create the speckles for the D.I.C. detection. Five series of samples of two different steels, whose material and size are illustrated in Table 1, were tested. Except the first two, the others series were shaped following the ASTM E606 standards.

The tests were performed by an Instron 8501 servohydraulic testing machine, two columns frame, and capacity up to 100 kN, with hydraulic wedge action grips for fatigue testing.

Two different thermocameras were used for the different tested series: a FLIR Thermacam A320, for the first two series, with a 18 mm lens, a spatial resolution of 320x240 pixels and a thermal sensitivity of 30 mK, and a FLIR SC3000, for the other series, with a 18 mm macro lens, a spatial resolution of 320x240 pixels and a thermal sensitivity of 20 mK. Both the thermocameras were able to acquire up to 60 frames/s.

A differential compensation methodology was applied, similarly to that used for the electrical strain gauges: a dummy compensator of the same material was mounted on the grips in parallel to the specimen but without loading them. The temperature of the dummy depends on the environmental conditions (ambient temperature, heat transfer from the grips, etc.), while that of the specimen depends also on the loading conditions. The thermal variations are corrected subtracting those of the dummy compensator to those of the specimen (Risitano et al. 2014).

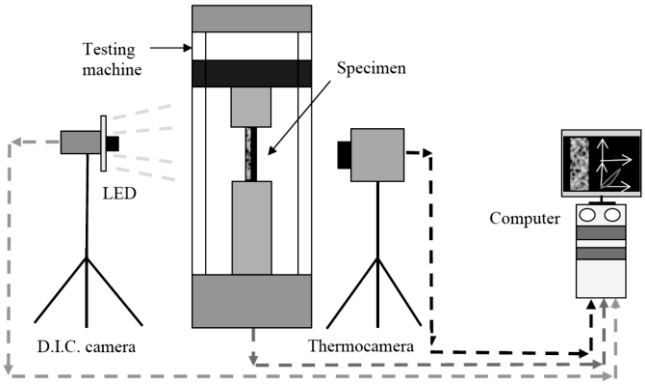

Figure 1. Scheme of the experimental setup.

Figure 2. Experimental setup.

Table 1. Material and size of the specimens.

Series	Material	Overall length [mm]	Thickness [mm]	Length of reduced section [mm]	Width of grip section [mm]	Width of reduced section [mm]	Fillet radius [mm]
1	AISI 304	200	4.1	100	20	10.4	40
2	AISI 304	200	5.0	85	20	10.2	12
3	AISI 304	189	6.5	35	32	16	13
4	AISI 304	189	5.0	35	32	16	13
5	EN 10025	189	5.0	35	32	16	13

The D.I.C. image sequences were acquired using an Image Source DMK 23G445 monochromatic videocamera equipped with a ¼" Sony CCD ICX098BL sensor, a 35 mm lens, extension rings and a specific ring of LED to assure a correct light distribution without interferences with the image acquisition system (La Rosa et al. 2016 and 2017).

Particular carefulness was considered to synchronize the images in the processing. The experimental setup was modified, introducing a device able to acquire contemporaneously all the data from the D.I.C. camera as well as from the load cell and from the displacement sensor of the testing machine, by inserting an acquisition board NI PXIe-1073 coupled to a PC with NI LabVIEW software. The program, developed in LabVIEW, acquires force and displacement data from the machine and a single frame of the specimen at a given instant and proceeds to the acquisition of 33 samples at a sample rate of 1 kHz for each image. Therefore, the software acquires the frames and, between two consecutive acquisitions, calculates the average of the 33 values, which takes as best value, and determines the standard deviation of the series. Thus, the synchronization error is reduced to 1/30 s, corresponding to the phase shift of a single frame, while the displacement signal is less subject to fluctuation errors due to electronic noise (Wattrisse et al. 2001, Li et al. 2016). A key element of the developed software (shown in Figure 3) allows generating the video file from which you can acquire the individual frames at request. Finally, a filter cuts the frequencies higher to that of the applied load, therefore obtaining the hysteresis areas in a more correct form as shown in Figure 4.

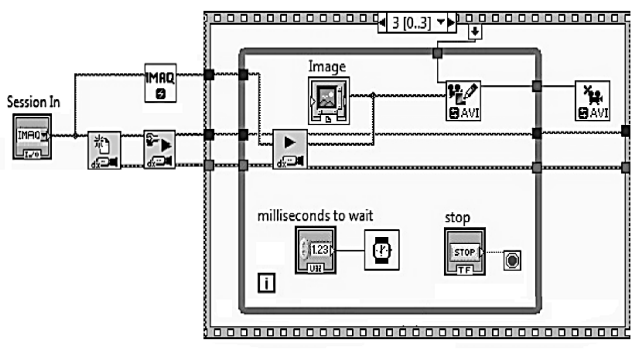

Figure 3. Block diagram of the acquisition program.

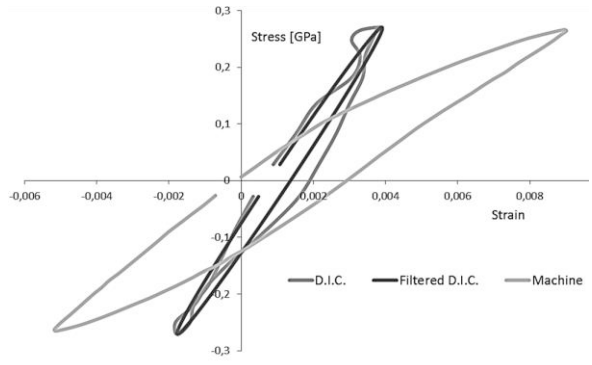

Figure 4. D.I.C. and filtered D.I.C. hysteresis areas compared with that derived from the testing machine (b).

Two different procedures were performed to test the samples: under displacement control and under loading control. The initial proposal tended to perform the analysis under displacement control, easy to carry out by the testing machines. Then, the first series was initially tested under monotonic displacement control, programming 10 steps of increasing average displacement and peak-to-peak cyclic amplitude, being each step a train of 100 sinusoidal oscillations. The steps were applied in sequence, with interval of 1 second between them, during which the load was nil before starting with the new pulse train. The frequency was maintained low (1 Hz), in order to acquire a sufficient number of images for cycle to be processed by D.I.C., using a frame rate of 30 fps.

The purpose was to produce tensile stresses only. On the contrary, the loading induced on the specimens tended to produce compressive stresses after the first steps, caused by the testing machine clearances and by the plastic residual deformations. The hysteresis cycles reported in Figure 5 highlight the different phenomena of compressive load (since the forth step), increasing their area and strain ratcheting (Sarkar et al. 2016, Mukopadhyay et al. 2014).

The following series, therefore, were tested under loading control. The second series was tested with a loading ratio R=0. Also in this case, however, clearances and the plastic deformations still affect the tests and make little reliable evidence from the energy point of view. The other series (3 to 5) were tested with loading ratio R=-1. Figure 6 shows the strain derived from the data furnished by the testing machine together with that derived by the D.I.C. for the sequence of applied loading of the series 4. It is evident the considerable difference between the two measurements, which show a scale factor of the order of about 2÷3:1.

The area of the hysteresis cycle was calculated in three moments per step: at the beginning (20th cycle) in the mean point (50th cycle) and before the end (80th cycle). The computation was made using an algorithm in Excel cumulating trapezoidal areas for each measurement point (30 per cycle) considering increasing and decreasing phases of strain.

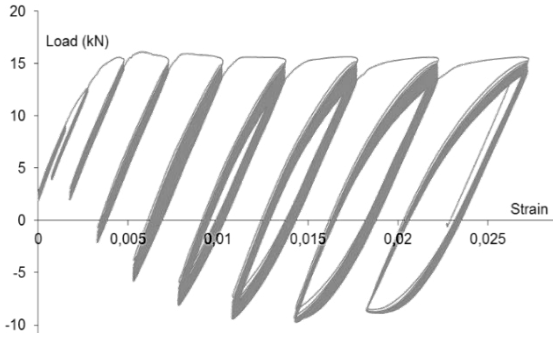

Figure 5. Hysteresis and ratcheting produced in the test series 1

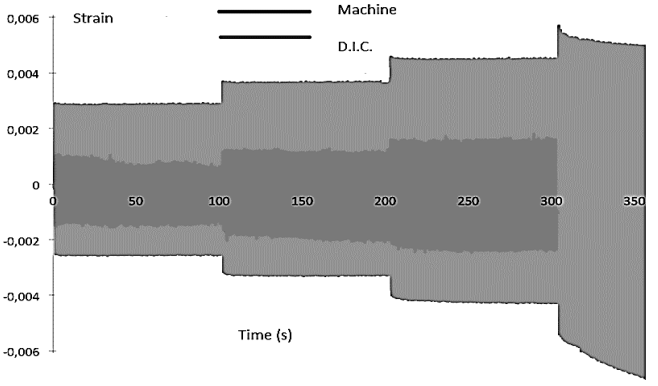

Figure 6. Cyclic loading for series 4 by the testing machine or by the DIC

3. Analysis of results

As well known by the literature on the thermographic analysis, in fatigue conditions the temperature variations growth in the first phase with the increased cyclic load over the fatigue limit. This phenomenon is induced by the local microplasticity linked to the crack nucleation and propagation. The thermal increments are proportional to the applied frequency and reach the stabilization temperature after some hundreds or thousands of cycles (La Rosa and Risitano 2000). The low frequency (1 Hz) leads to modest values of temperature increases.

The more interesting results can be achieved by the tests under loading control with R=-1 (series 3 to 5). As an example, the thermal increments detected in the tests of the series 5 are shown (Figure 7). A similar behavior was found for all the three series tested, obviously with different amount of the mean thermal increments. Comparing the curves of the energy and the thermal variations of the same series (first three steps), it is possible to notice a good agreement between them in the elastic zone, highlighting how the thermal behavior is representative of the energy dissipation.

Finally, in Figure 8, the phase angle between stress and strain either measured by the testing machine parameters or by the D.I.C. is reported. The angle is almost stable and relatively small in the first three steps, even if growing with the applied load. The values are quite limited, between 2 and 6 deg in the elastic zone, as expected from this material. Its increase rapidly in the fourth step, demonstrating again that the material is subjected to plastic behavior. The angle values measured by the D.I.C. and those derived by the testing machine have the same behavior but the former are higher. In fact, considering that the hysteresis area A can be written as:

$$A = \sigma_0 \, \varepsilon_0 \, \pi \sin(\varphi) \tag{1}$$

the ratio between the hysteresis areas can be approximated as:

$$\frac{A_{DIC}}{A_{mach}} = \frac{\sigma_0}{\sigma_0} \frac{\varepsilon_{0DIC}}{\epsilon_{0mach}} \frac{\pi}{\pi} \frac{\sin \varphi_{DIC}}{\sin \varphi_{mach}} \sim \frac{\varepsilon_{0DIC}}{\varepsilon_{0mach}} \frac{\varphi_{DIC}}{\varphi_{mach}} \tag{2}$$

The term A_{DIC}/A_{mach} is of the order of 1/1.5 while the strains ratio $\varepsilon_{0DIC}/\varepsilon_{0mach}$ is quite lower, of the order of 1/(2÷3) due the high difference between the strain detected by D.I.C. (ε_{0DIC}) and that revealed by the testing machine (ε_{0mach}), even if with the same behavior. Then, it is reasonable that the phase angles ratio ϕ_{DIC}/ϕ_{mach} is of the order of 1.5 and that ϕ_{DIC} and ϕ_{mach} could have the same behavior.

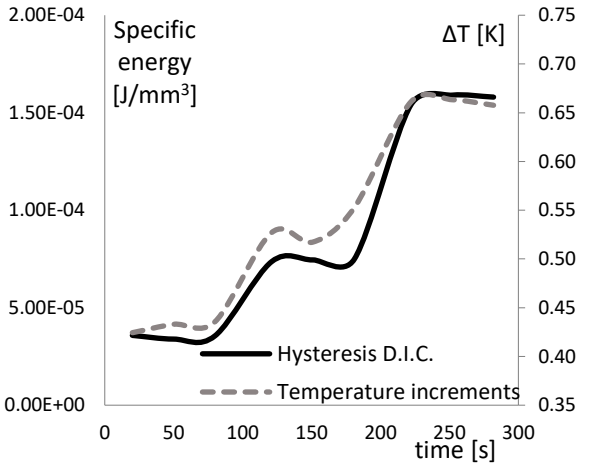

Figure 7. Comparison between thermal increments and specific energy calculated by D.I.C.

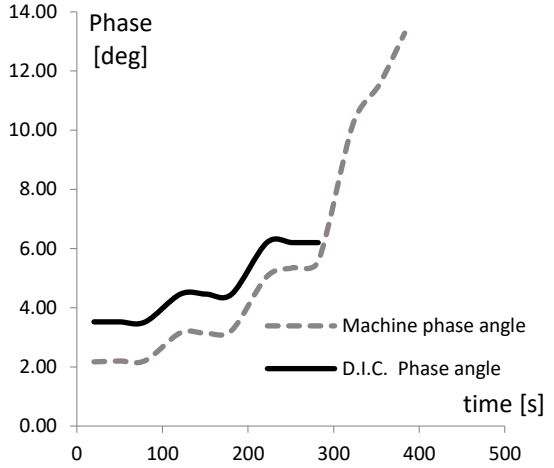

Figure 8. Phase angle between stress and strain calculated by the machine parameters and the D.I.C.

4. Conclusions

The authors have performed different series of tests to compare the energy measured by the hysteresis area with that detected using the thermography on specimens subjected to trains of increasing cyclic loading. Thermal and D.I.C. measurements were carried out at the same time on both the sides of the specimens, on purpose painted to increase the emissivity (for a better thermography analysis) and to generate the speckles (to perform the D.I.C.).

After the first unsatisfying trials under displacement control and load control with R=0, the authors have focused their attention on tests under load control with R=-1. Particular care was devoted to the synchronization of the images.

The displacements were measured using the D.I.C. method, in order to avoid any errors due to clearances or rigid displacements of the measuring chain. The comparison among the displacements obtained by the D.I.C. analysis with those furnished by the testing machine parameters shows similar behavior but different amounts, with ratios of the order of 1:(2÷3). Likewise, the damping angles have a similar behavior with different values.

The comparison between the specific energy dissipated, calculated using the D.I.C., and detected, by the thermal increments of some spots on the specimens, highlight a good qualitative agreement, encouraging the authors to a deeper quantitative analysis.

References

Audenino, A.L., Crupi, V., Zanetti, E.M. (2003) Correlation between thermography and internal damping in metals, International Journal of Fatigue, 25, 4, 343-351.

Boulanger T., Chrysochoos A., Mabru C., Galtier A. (2004) Calorimetric analysis of dissipative and thermoelastic effects associated with the fatigue behavior of steels, International Journal of Fatigue 26, 221–229.

Charkaluk E., Constantinescu A. (2009) Dissipative aspects in high cycle fatigue, Mechanics of Materials 41 483–494.

Crupi V., Chiofalo G., Guglielmino E. (2010) Using infrared thermography in low-cycle fatigue studies of welded joints, Welding Journal 89, 195-200.
Crupi V., Chiofalo G., Guglielmino E. (2011) Infrared investigations for the analysis of low cycle fatigue processes in carbon steels, Journal of Mechanical Engineering Science, Proceedings of the Institution of Mechanical Engineers Part C, Vol. 225, n. 4, 833-842.
Curà F., Gallinati A.E. (2011) Fatigue damage identification by means of modal parameters, Procedia Engineering, 10, 1697–1702.
Dattoma V., Giancane S. (2013) Evaluation of energy of fatigue damage into GFRC through digital image correlation and thermography Composites: Part B 47, 283–289.
Fargione G., Geraci A., La Rosa G., Risitano A. (2002) Rapid Determination of the Fatigue Curve by Thermographic Method, International Journal of Fatigue, 24, 11-19.
Felter C.E., Morrow J.D. (1961) Microplastic strain hysteresis energy as a criterion for fatigue fracture, J. Basic. Eng. 83, 15-22.
Giancane S., Chrysochoos A., Dattoma V, Wattrisse B. (2009) Deformation and dissipated energies for high cycle fatigue of 2024-T3 aluminium alloy, Theoretical and Applied Fracture Mechanics 52, 117–121.
Giancane S., Panella F.W., Nobile R., Dattoma V. (2010) Fatigue damage evolution of fiber reinforced composites with digital image correlation analysis Procedia Engineering 2, 1307–1315.
Grover H. J. (1960) An observation concerning the cycle ratio in cumulative damage, Proc. Fatigue in Aircraft Structures ASTM STP 274, Philadelphia, 120–124.
Hunady R., Hagara M., Schrötter M. (2012) Using high-speed digital image correlation to determine the damping ratio, MMaMS 2012 Procedia Engineering 48, 242–249.
Kaleta J., Blotny R., Harig H. (1990) Energy stored in a specimen under fatigue limit loading conditions. J. Test Eval., 19, 326–333.
Kanchanomai C., Yamamoto S., Miyashita Y., Mutoh Y., McEvily A.J. (2002) Low cycle fatigue test for solders using non-contact digital image measurement system, International Journal of Fatigue 24, 57–67.
La Rosa G., Risitano A. (2000) Thermographic methodology for rapid determination of the fatigue limit of materials and mechanical components, International Journal of Fatigue. Vol. 22, 65-73.
La Rosa, G., Clienti, C., Lo Savio, F. (2014) Fatigue analysis by acoustic emission and thermographic techniques. Procedia Engineering, 74, 261-268.
La Rosa G., Clienti C., Marino Cugno Garrano A. (2016) The use of digital image correlation to correct the thermoelastic curves in static tests. Structural Integrity Procedia, 2, 2140-2147.
La Rosa G., Clienti C., Marino Cugno Garrano A., Lo Savio F. (2017) A novel procedure for tracking the measuring point in thermoelastic curves using D.I.C. Engineering Fracture Mechanics, 183, 53-65.
Li L., Muracciole J.M., Waltz L., Sabatier L., Barou F., Wattrisse B. (2016) Local experimental investigations of the thermomechanical behavior of a coarse-grained aluminum multicrystal using combined DIC and IRT methods, Optics and Lasers in Engineering, 8, 1–10.
Luong M.P. (1988) Fatigue limit evaluation of metals using an infrared thermographic technique, Mech. Mater., 28, 155-163.
Meneghetti G., Ricotta M., Atzori B. (2013) A synthesis of the push-pull fatigue behaviour of plain and notched stainless steel specimens by using the specific heat loss, Fatigue & Fracture of Eng. Mat. & Struct., Wiley Online Library.
Mukhopadhyay C.K., Jayakumar T., Haneef T.K., Suresh Kumar S., Rao B.P.C., Goyal S., Gupta S.K., Bhasin V., Vishnuvardhan S., Raghava G., Gandhi P. (2014) Use of acoustic emission and ultrasonic techniques for monitoring crack initiation/growth during ratcheting studies on 304LN stainless steel straight pipe, International Journal of Pressure Vessels and Piping 116, 27-36.
Naderi M., Amiri M., Khonsari M. M. (2010) On the thermodynamic entropy of fatigue fracture, Proc. R. Soc. A 466, 423-438.
Plekhov O. A., Saintier, N., Palin-luc, T., Uranov, S. V. and Naimark, O. (2007) Theoretical analysis, infrared and structural investigations of energy dissipation in metals under cyclic loading. Mater. Sci. Eng., 462, 367–369.
Risitano A., Risitano G. (2010) Cumulative damage evaluation of steel using infrared thermography, Theor. Appl. Fract. Mech., 54, 82-90.
Risitano A., Risitano G. (2013) Cumulative damage evaluation in multiple cycle fatigue tests taking into account energy parameters, International Journal of Fatigue, 48, 4, 214–222.
Risitano A., Fargione G., Clienti C. (2014) Caratterizzazione a fatica di bulloni in acciaio basata sul rilascio termico sotto stati di tensione, 43th National Conference of the AIAS (Italian Association for the Stress Analysis), Bologna, Italy, 9-12 September 2014 (in italian).
Risitano A., La Rosa G., Geraci A., Guglielmino E. (2015) The choice of thermal analysis to evaluate the monoaxial fatigue strength on materials and mechanical components, Proceedings of the Institution of Mechanical Engineers, Part C: Journal of Mechanical Engineering Science 229, 7, 19, 1315-1326.
Roy S:C:, Goyal S., Sandhya R., Ray S. K. (2013) Analysis of hysteresis loops of 316l(n) stainless steel under low cycle fatigue loading conditions, Procedia Engineering 55, 165–170.
Sarkar A., Nagesha A., Parameswaran P., Sandhya R., Mathew M.D. (2013) Influence of dynamic strain aging on the deformation behavior during ratcheting of a 316LN stainless steel, Materials Science & Engineering A 564, 359–368.
Sarkar A., De P.S., Mahato J.K., Kundu A., Chakraborti P.C. (2014) Effect of mean stress and solution annealing temperature on ratcheting behaviour of AISI 304 Stainless Steel, Procedia Engineering XVII Int. Colloquium on Mechanical Fatigue of Metals (ICMFM17),74, 376–383.
Tao G., Xia Z. (2005) A non-contact real-time strain measurement and control system for multiaxial cyclic/fatigue tests of polymer materials by digital image correlation method, Polymer Testing 24, 844–855.
Wattrisse B., Chrysochoos A., Muracciole J.M., Némoz-Gaillard M. (2001) Kinematic manifestations of localisation phenomena in steels by digital image correlation, European Journal of Mechanics - A/Solids, 20, 2, 189-211.